Optik 159 (2018) 31–38

Contents lists available at ScienceDirect

Optik

journal homepage: www.elsevier.de/ijleo

Original research article

Data inversion method for dual-frequency Doppler lidar based on Fabry-Perot etalon quad-edge technique

Wenxin Guo[a], Fahua Shen[a,*], Wenjuan Shi[a], Mengling Liu[a], Yingying Wang[a], Chengyun Zhu[a], Liujing Shen[a], Bangxin Wang[b], Peng Zhuang[b]

[a] Department of New Energy and Electronic Engineering, Yancheng Teachers University, 2 Hope Avenue South Road, Yancheng, Jiangsu 224007, China

[b] Key Laboratory of Atmospheric Optics, Anhui Institute of Optics and Fine Mechanics, Chinese Academy of Sciences, 350 Shushanghu Road, Hefei, Anhui 230031, China

ARTICLE INFO

Article history:
Received 21 December 2017
Accepted 13 January 2018

Keywords:
Doppler lidar
Fabry-Perot etalon
Quad-edge technique
Dual frequency
Wind
Backscatter ratio

ABSTRACT

In order to realize the accurate inversion of lidar data, the calibration method for the ratio of Fabry-Perot etalon (FPE) transmission to reflection curve is given, and the reliability of the method is verified by simulation test. The effective ratio of FPE transmission to reflection for the actual atmospheric detection is analyzed, and a nonlinear iterative algorithm for simultaneous inversion of wind field and backscatter ratio, as well as the specific iterative steps, initial value determination methods and corresponding error formula of parameters are proposed. The simulation results show that no matter whether the backscatter ratio R_β is small or large, the iterative process is always convergent and the correct inversion results can be obtained. The value of R_β has a great influence on the convergence rate of its own, but has little effect on the wind speed convergence rate. The smaller R_β is, the faster convergence rate of R_β is, vice versa. Error analysis inferred that under the shot-noise limit, the radial wind speed measurement error decreases rapidly with the increase of R_β for $1 < R_\beta < 2$, decreases slowly with the increase of R_β for $R_\beta > 2$; if the total number of backscattering photons of 50,000 received by telescope is assumed, the backscatter ratio measurement error increases with the increase of R_β; within the wind speed measurement dynamic range of ±25 m/s, the radial wind speed error is below 2m/s and the backscatter ratio relative error is less than 4.1% when $1.1 < R_\beta < 10$.

1. Introduction

High-precision, high spatial and temporal resolution real-time wind field data is of great importance for improving climate models, studying global climate change, promoting atmospheric thermodynamics and kinetics, improving the accuracy of weather forecasts, ensuring aircraft takeoff and landing safety, improving the utilization of wind energy and so on. Therefore, as one of the most effective tools for wind field detection, Doppler lidar has been deeply researched and developed rapidly, and has formed direct-detection system [1–6] and coherent system [7,8]. On the basis of the traditional double-edge detection technique, the author proposed a dual-frequency Doppler lidar based on FPE quad-edge technique. Compared with the traditional double-edge detection Doppler lidar, this lidar can effectively improve the wind detection performance [9,10].

* Corresponding author.
E-mail address: sfh81914@163.com (F. Shen).

https://doi.org/10.1016/j.ijleo.2018.01.035
0030-4026/

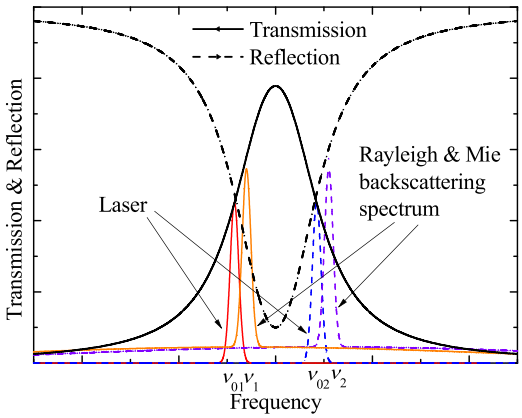

Fig. 1. Wind measurement principle based on F–P etalon quad-edge and dual-frequency technique.

However, the final performance of the lidar system not only depends on the hardware, but also the data inversion method. Whether the data inversion method is correct and effective is very important. Based on the analysis of the measurement principle and system structure of this dual frequency Doppler lidar, the data inversion problems of the system, including system calibration, parameter inversion and corresponding measurement errors, are studied in depth.

2. Measurement principle and system structure

As shown in Fig. 1, the transmission and reflection spectrum of FPE are intersected at the two waist. Two frequencies of the outgoing laser ν_{0i} ($i = 1, 2$) are locked in the vicinity of these two intersection points respectively to form the dual-frequency four-edge detection technique [9]. The outgoing laser is emitted into the atmosphere and is scattered by atmospheric molecules and aerosol particles with a macro velocity (wind speed). The backscattered light will have Doppler frequency shift and the amount of frequency shift is $\nu_d = \nu_i - \nu_{0i} = 2V_r/\lambda$, where ν_i ($i = 1, 2$) is the frequency of backscattered light, V_r is radial wind speed, λ is laser wavelength. Then, the transmittance and reflectance of the backscattered light passing through the FPE will change accordingly. The magnitude and direction of the radial wind speed can be derived from the pre-calibrated transmission and reflection curve of FPE and the measured change in transmittance and reflectance.

Fig. 2 shows the structure of dual-frequency Doppler lidar system based on FPE quad-edge technique [10]. The transmitting system adopts a narrow-linewidth and frequency stabilization tunable semiconductor laser with MOPA structure at 852 nm, and the transmitting laser frequency is changed alternately between ν_{01} and ν_{02} by using an acousto-optic frequency shifter. The transmitting laser is split into two beams by a beam splitter (T/R = 99/1). The reflected light is coupled by a branch of the 1×2 multimode fiber coupler A into a 100 m long fiber, whose backscattered light is used as reference and enters one branch of the 1×2 multimode fiber coupler B through the other branch of coupler A. The transmitted light passes through a beam expander, two reflectors and a two-dimensional scanner sequentially, and then enters into the atmospheric detection area with a preset angle. The atmospheric backscattered light is received by a telescope and then passes through a narrow-band interference filter to suppress the sky background light. After a 200 m long fiber delay, it enters the other branch of coupler B. The optical signal coming out from the combine of coupler B enters into a collimator through the $1 \rightarrow 2$ path of an optical circulator, and the collimated light beam is incident on the FPE. The optical signal passing through the FPE is converged through a convex lens, coupled to the photon counting detector APD1 by an optical fiber; the optical signal reflected by the FPE is converged in the reverse direction through the collimator, passes through the $2 \rightarrow 3$ path of the optical circulator and then is coupled to the photon counting detector APD2. The output signals of the two detectors are acquired by a dual-channel photon counting card, and then processed by an IPC for data processing, storage, inversion and result display. The system's laser, acousto-optic shifter, two-dimensional scanner, photon counting card and so on are all controlled by the IPC through the RS232 serial port.

3. Calibration of the ratio function of FPE's transmission to reflection

3.1. The ratio function of FPE's transmission to reflection

The transmission and reflection of the beam with Gaussian spectral distribution, uniform light intensity and full divergence angle of $2\theta_0$ incident on the FPE are [9]:

$$\mathfrak{I}(\nu) = T_{av} M(\nu) \tag{1}$$

$$\Re(\nu) = 1 - A - C_0 \mathfrak{I}(\nu) \tag{2}$$

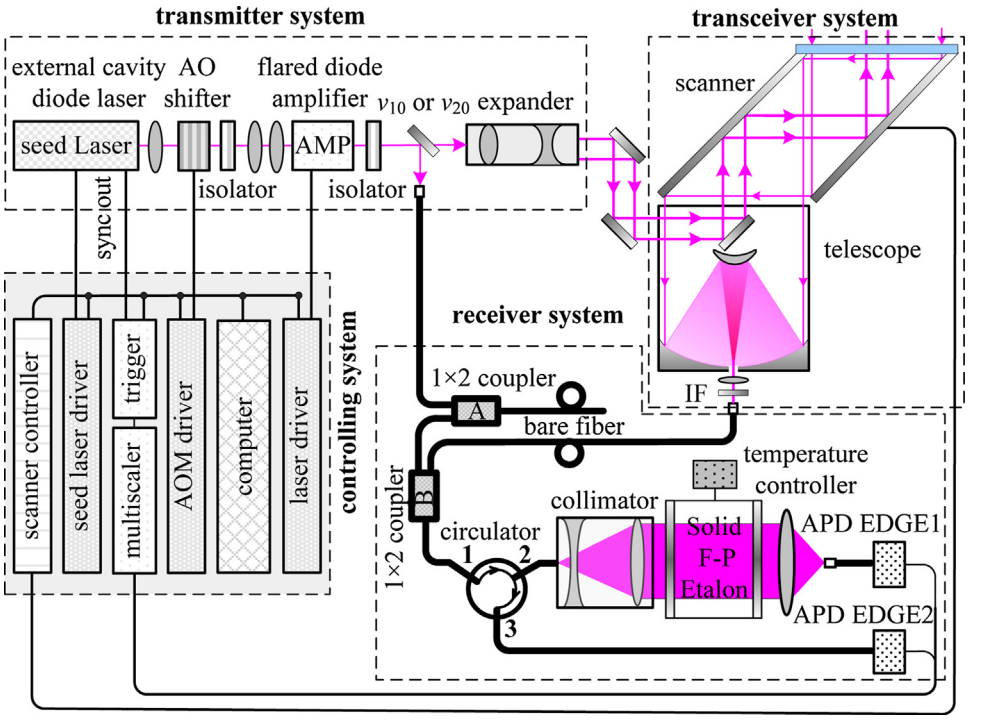

Fig. 2. The structure of dual frequency Doppler lidar system based on F–P etalon quad-edge technique.

where

$$M(\nu) = 1 + 2\sum_{m=1}^{\infty} R^m \cos\left[\frac{2\pi m\nu}{\nu_{FSR}}\left(1 - \frac{\Omega_{FP}}{4\pi}\right)\right] \cdot \exp\left[-\left(\frac{\pi m \Delta\nu_e}{\nu_{FSR}}\right)^2\right] \sin c\left(\frac{2m\nu}{\nu_{FSR}}\frac{\Omega_{FP}}{4\pi}\right)$$

where $T_{av} = (1\text{-}R\text{-}A)^2/(1\text{-}R^2)$ is the average transmittance of FPE, $C_0 = [1\text{-}R(1\text{-}A)]/(1\text{-}R\text{-}A)$, R is the FPE's plate reflectivity of corresponding wavelength, A accounts for any absorptive or scattering losses in the plates, ν_{FSR} is the free spectral spacing of FPE, $\Omega_{FP} = 2\pi(1\text{-}\cos\theta_0)$ is the solid angle of the incident beam, ν is the center frequency of incident light, $\Delta\nu_e$ is the 1/e width of the equivalent incident laser spectrum, including the contribution of incident spectral width and spectral broadening due to non-parallelism and surface defect of the two plates. For the outgoing laser or Mie backscattering light, $\Delta\nu_e = \Delta\nu_l$, $\Delta\nu_l$ is the 1/e width of the equivalent outgoing laser spectrum; for Rayleigh backscattering light, $\Delta\nu_e = (\Delta\nu_l{}^2 + \Delta\nu_r{}^2)^{1/2}$, where $\Delta\nu_r = (8kT_a/M\lambda^2)^{1/2}$, T_a is the atmospheric temperature, λ is the laser wavelength, k is the Boltzmann constant, M is the average mass of an atmospheric molecule. The ratio function of FPE's transmission to reflection is defined as

$$h(\nu) = \Im(\nu)/\Re(\nu) = \left[(1 - A)/\Im(\nu) - C_0)\right]^{-1} \tag{3}$$

3.2. Calibration method

Before the wind field measurement is carried out, the acousto-optic modulator driver does not input the modulation signal. By applying a linearly varying driving current to the seed laser of the tunable semiconductor laser, the laser frequency changes linearly and the reference light is used to scan the FPE to obtain the original data column $N_t(\nu_n)$ and $N_r(\nu_n)$, and we get

$$(1 - A)/\Im(\nu_n) - C_0 = N_r(\nu_n)/N_t(\nu_n) \tag{4}$$

where n is the number of steps in the frequency scanning, and ν_n is the corresponding transmitting laser frequency in step n. Since A is small, the following fitting equation is used for nonlinear fitting

$$f_{fit}(\nu) = 1/h_{fit}(\nu) = 1/\Im(\nu - \nu_p) + C \tag{5}$$

where C is a constant including the background and C_0, ν_p is the center frequency. The fitting parameters are FSR of FPE ν_{FSR}, reflectivity R, average transmittance T_{av} and center frequency ν_p. According to the Rogers criterion [11], if the relative error of the transmission is required below 0.1% and R is 0.89, the order of the transmission and reflection expressions $m \approx 30$. To ensure the fitting precision, take $m = 50$. An example of a fitting is as follows. The initial values are set as $\nu_{FSR} = 3.5$GHz, $R = 0.886$, $T_{av} = 0.0594$ and $\nu_p = 0$. During the calibration process, the number of reference photons incident on FPE is assumed

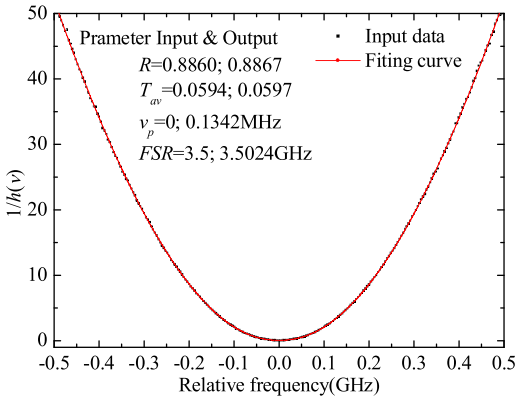

Fig. 3. The results of nonlinear least squares fitting of $1/h(\nu)$.

to be 10^6 (average) for measuring single scanning point and the frequency scanning step is 4MHz. Then, we use the Monte-Carlo method to simulate the signal $N_r(\nu_n)$, $N_t(\nu_n)$ and the nonlinear least square fitting method to fit the data. The fitting values of the parameters are ν_{FSR} = 3.5024GHz, R = 0.8867, T_{av} = 0.0597 and ν_p = 0.1342MHz, which are very close to the input values, as shown in Fig. 3. The fitting parameter values are brought into the transmission and reflection expressions, the experimental calibrated FPE's transmission and reflection functions can be obtained.

4. Data processing method

4.1. The effective ratio function of FPE's transmission to reflection

The atmospheric backscatter signal contains the aerosol backscatter signal and the atmospheric molecular backscatter signal. Then, after the backscattered light with the center frequency of $\nu_{0i} + \nu_d$ is incident on the FPE, the transmitted signal into APD1 and the reflected signal into APD2 can be respectively expressed as

$$N_t(\nu_{0i} + \nu_d, T_a) = N_{ai}\Im^{(a)}(\nu_{0i} + \nu_d) + N_{mi}\Im^{(m)}(\nu_{0i} + \nu_d, T_a) \tag{6}$$

$$N_r(\nu_{0i} + \nu_d, T_a) = N_{ai}\Re^{(a)}(\nu_{0i} + \nu_d) + N_{mi}\Re^{(m)}(\nu_{0i} + \nu_d, T_a) \tag{7}$$

where i = 1, 2; N_{ai} and N_{mi} are the aerosol scattering signal and the molecular scattering signal respectively in the backscattering signal of center frequency $\nu_{0i} + \nu_d$. The total backscattering signal is $N_i = N_{ai} + N_{mi}$, T_a is the atmospheric temperature.

In a single measurement cycle, the composition of the atmosphere can be considered stable with a backscattering ratio of $R_\beta = 1 + \beta_a/\beta_r$, where β_a and β_r are the atmospheric backscatter coefficients for aerosols and molecules, respectively, Then we have

$$R_\beta = 1 + N_{ai}/N_{mi} \tag{8}$$

Thus, Eq. (6) and Eq. (7) can be expressed as

$$N_t(\nu_{0i} + \nu_d, T_a, R_\beta) = N_i\Im_e(\nu_{0i} + \nu_d, T_a, R_\beta) \tag{9}$$

$$N_r(\nu_{0i} + \nu_d, T_a, R_\beta) = N_i\Re_e(\nu_{0i} + \nu_d, T_a, R_\beta) \tag{10}$$

where $\Im_e$ and $\Re_e$ are defined as the effective transmission and reflection functions, whose forms are same as Eqs. (1) and (2), and can be obtained by simply replacing $M(\nu)$ with the following $M_e(\nu)$ expression

$$M_e(\nu, T_a, R_\beta) = 1 + 2\sum_{m=1}^{\infty} R^m \cos\left[\frac{2\pi m\nu}{\nu_{FSR}}\left(1 - \frac{\Omega_{FP}}{4\pi}\right)\right] \cdot \exp\left[-\left(\frac{\pi m\Delta\nu_l}{\nu_{FSR}}\right)^2\right] \sin c\left(\frac{2m\nu_0}{\nu_{FSR}}\frac{\Omega_{FP}}{4\pi}\right)$$
$$\left\{1 + \frac{1}{R_\beta}\left\{\exp\left[-\left(\frac{\pi m}{\nu_{FSR}}\right)^2\frac{8kT_a}{M\lambda^2}\right] - 1\right\}\right\}$$

The effective ratio function of FPE's transmission to reflection is defined as

$$h_e(\nu_{0i} + \nu_d, T_a, R_\beta) = \frac{N_t(\nu_{0i} + \nu_d, T_a, R_\beta)}{N_r(\nu_{0i} + \nu_d, T_a, R_\beta)} = \frac{\Im_e(\nu_{0i} + \nu_d, T_a, R_\beta)}{\Re_e(\nu_{0i} + \nu_d, T_a, R_\beta)} \tag{11}$$

In this paper, the FWHM of FPE, the 1/e width of the equivalent outgoing laser spectrum $\Delta\nu_l$, FPE's plate absorption A, atmospheric temperature T_a and the full divergence angle of incident beam $2\theta_0$ are assumed to be 135MHz, 37MHz, 0.1%, 280K and 1mrad respectively. Fig. 4 shows the effective ratio function of FPE's transmission to reflection for different

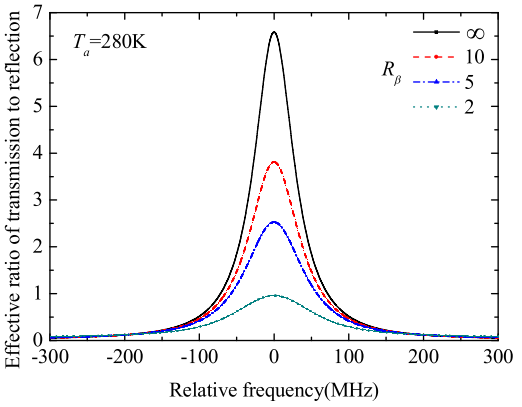

Fig. 4. Effective ratio of FPE's transmission to reflection for atmospheric backscattering light with differentR_β.

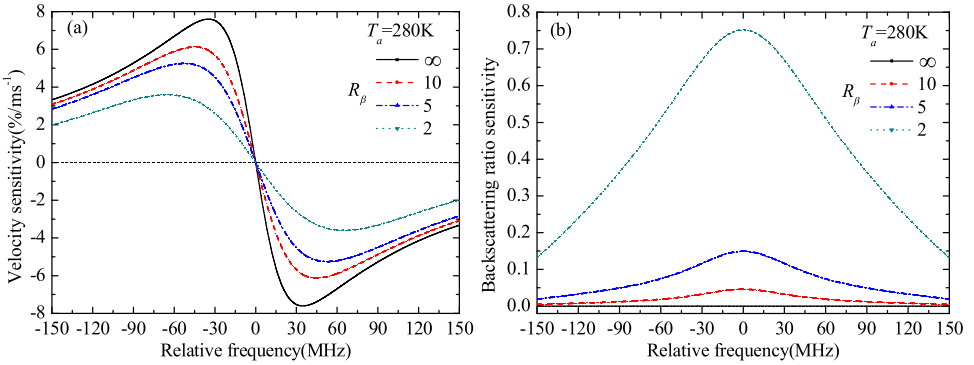

Fig. 5. θ_V and θ_R vary with frequency for different backscatter ratios.

backscatter ratios. As can be seen from Fig. 4, the effective ratio function curve of FPE's transmission to reflection decreases sharply as the backscatter ratio decreases.

4.2. Simultaneous inversion method of wind field and backscatter ratio

Because of adopting the dual frequencies, the nonlinear equations of two functions $h_e(\nu_{10}+\nu_d, T_a, R_\beta)$ and $h_e(\nu_{20}+\nu_d, T_a, R_\beta)$ can be obtained according to Eq. (11)

$$\begin{cases} h_e(\nu_{01}+\nu_d, T_a, R_\beta) - N_t(\nu_{01}+\nu_d, T_a, R_\beta)/N_r(\nu_{01}+\nu_d, T_a, R_\beta) = 0 \\ h_e(\nu_{02}+\nu_d, T_a, R_\beta) - N_t(\nu_{02}+\nu_d, T_a, R_\beta)/N_r(\nu_{02}+\nu_d, T_a, R_\beta) = 0 \end{cases} \tag{12}$$

The Taylor expansion is carried out on Eq. (12) and retained to the first order, one can get

$$\begin{pmatrix} \dfrac{\partial h_e(\nu_{01}+\nu_d^{(j)}, T_a, R_\beta^{(j)})}{\partial V_r} & \dfrac{\partial h_e(\nu_{01}+\nu_d^{(j)}, T_a, R_\beta^{(j)})}{\partial R_\beta} \\ \dfrac{\partial h_e(\nu_{02}+\nu_d^{(j)}, T_a, R_\beta^{(j)})}{\partial V_r} & \dfrac{\partial h_e(\nu_{02}+\nu_d^{(j)}, T_a, R_\beta^{(j)})}{\partial R_\beta} \end{pmatrix} \begin{pmatrix} v_r^{(j)} - v_r^{(j-1)} \\ R_\beta^{(j)} - R_\beta^{(j-1)} \end{pmatrix} = \begin{pmatrix} \dfrac{N_t(\nu_{01}+\nu_d, T_a, R_\beta)}{N_r(\nu_{01}+\nu_d, T_a, R_\beta)} - h_e(\nu_{01}+\nu_d^{(j)}, T_a, R_\beta^{(j)}) \\ \dfrac{N_t(\nu_{02}+\nu_d, T_a, R_\beta)}{N_r(\nu_{02}+\nu_d, T_a, R_\beta)} - h_e(\nu_{02}+\nu_d^{(j)}, T_a, R_\beta^{(j)}) \end{pmatrix} \tag{13}$$

where $\nu_d^{(j)} = 2V_r^{(j)}/\lambda, j = 1,2,3\ldots$. The wind speed sensitivity and the backscatter ratio sensitivity of the effective ratio of FPE's transmission to reflection are defined as

$$\theta_V = (1/h_e)\partial h_e/\partial V_r \tag{14}$$

$$\theta_R = (1/h_e)\partial h_e/\partial R_\beta \tag{15}$$

Fig. 5(a) and (b) show the wind speed sensitivity and the backscatter ratio sensitivity vary with frequency for different backscatter ratios, respectively. Assuming that the initial outgoing laser frequencies ν_{01} and ν_{02} are locked at ± 72MHz from the center frequency of FPE respectively, the curves of total wind speed sensitivity and backscatter sensitivity versus radial

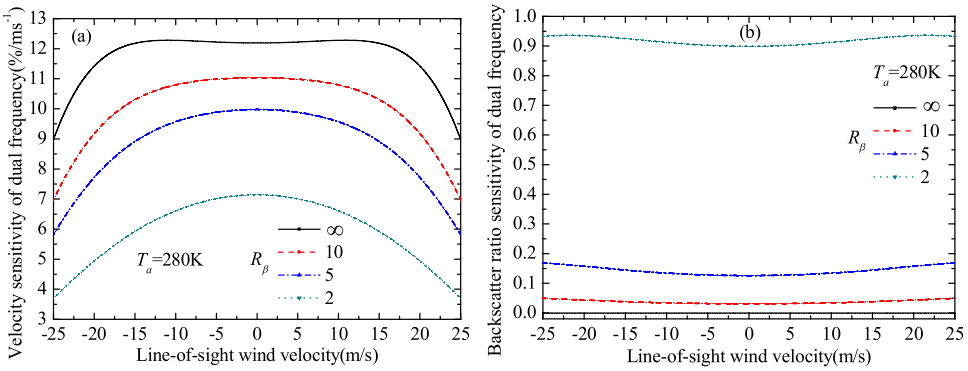

Fig. 6. Total wind speed sensitivity and backs catter ratio sensitivity vs LOS wind speed with double frequencies.

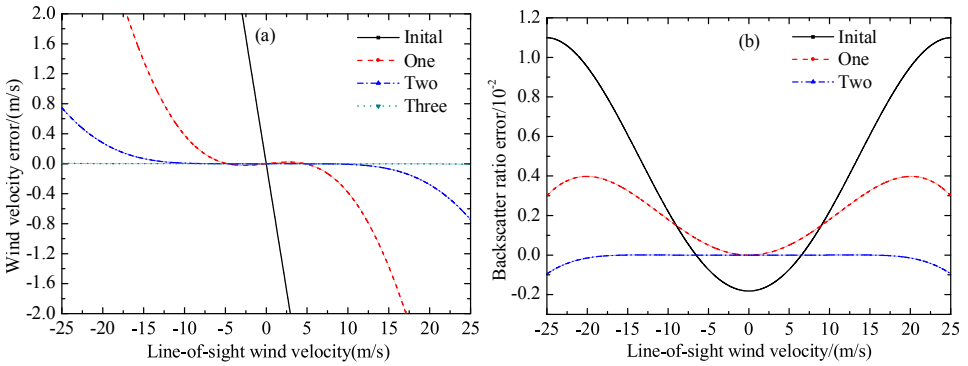

Fig. 7. WhenR_β = 1.1, the inversion results using nonlinear iteration method (a) radial wind speed; (b) backscatter ratio.

wind speed for dual frequency detection are shown in Fig. 6. As shown in Fig. 6, the greater the backscatter ratio is, the higher the wind speed sensitivity is, and the lower the backscatter ratio sensitivity is in the case of constant radial wind speed.

Let $h_{ei} = N_t(v_{0i} + v_d, T_a, R_\beta)/N_r(v_{0i} + v_d, T_a, R_\beta)$, $\theta_{Vi}^{(j)} = \theta_V(v_{0i} + v_d^{(j)}, T_a, R_\beta^{(j)})$, $\theta_{Ri}^{(j)} = \theta_R(v_{0i} + v_d^{(j)}, T_a, R_\beta^{(j)})$, $h_{ei}^{(j)} = h_{ei}(v_{0i} + v_d^{(j)}, T_a, R_\beta^{(j)})$, then Eq. (13) becomes

$$\begin{pmatrix} \theta_{V1}^{(j)} & \theta_{R1}^{(j)} \\ \theta_{V2}^{(j)} & \theta_{R2}^{(j)} \end{pmatrix} \begin{pmatrix} V_r^{(j)} - V_r^{(j-1)} \\ R_\beta^{(j)} - R_\beta^{(j-1)} \end{pmatrix} = \begin{pmatrix} h_{e1}/h_{e1}^{(j)} - 1 \\ h_{e2}/h_{e2}^{(j)} - 1 \end{pmatrix} \tag{16}$$

The specific iteration steps are as follows:

1) Setting the value of T_a according to the standard atmosphere model and the day's surface temperature; using the calibrated FPE's transmission and reflection functions obtained in Section 3.2 and h_{e1}, h_{e2} obtained from the wind measurement by lidar system, the iterative initial wind speed $V_r{}^{(0)}$ is obtained by means of the mean value method [12]; the $v_d{}^{(0)}$ and v_{10}, v_{20} measured by the reference light are taken into Eq. (12) to obtain $h_{e1}^{(0)}(R_\beta) + h_{e2}^{(0)}(R_\beta) = h_{e1} + h_{e2}$, then the initial backscatter ratio $R_\beta{}^{(0)}$ is obtained by interpolation method.
2) Substituting T_a, $V_r{}^{(0)}$ and $R_\beta{}^{(0)}$ into Eq. (16) yields $V_r{}^{(1)}$ and $R_\beta{}^{(1)}$.
3) Calculating $\delta V_r = V_r{}^{(j)} - V_r{}^{(j-1)}$ and $\delta R_\beta = R_\beta{}^{(j)} - R_\beta{}^{(j-1)}$ and setting the error limits ε_V and ε_R, judging whether the conditions $|\delta V_r| < \varepsilon_V$ and $|\delta R_\beta| < \varepsilon_R$ are both satisfied. If the conditions are not satisfied, repeat steps 2) and 3) until the condition satisfies, and stop the iteration. The obtained $V_r{}^{(j)}$ and $R_\beta{}^{(j)}$ are the final solved radial wind speed and backscatter ratio.

Assume T_a = 280K, R_β is taken as 1.1 and 10, ε_V is set to10^{-2}m/s, ε_R is set to 10^{-2}, within the wind speed dynamic range of ± 25m/s, the inversion results using the above iterative method are shown in Fig. 7 and Fig. 8, respectively. It can be seen that when R_β = 1.1, the inversion errors of the wind speed and the backscatter ratio will meet the accuracy requirements after three and two iterations respectively; when R_β = 10, the inversion errors of the wind speed and the backscatter ratio will meet the accuracy requirements after three and four iterations respectively. No matter whether the backscatter ratio is small or large, the iteration always converges and good inversion results can be obtained. The magnitude of the backscatter ratio has a great influence on the convergence speed of the backscatter ratio and has little effect on the convergence speed of

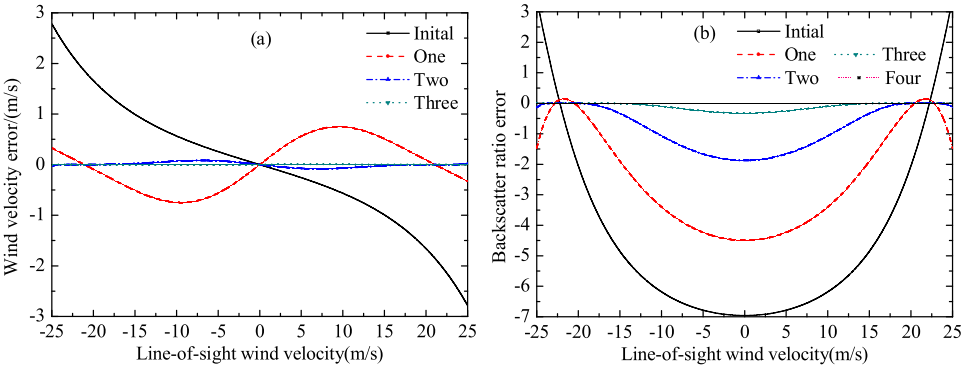

Fig. 8. WhenR_β = 10, the inversion results using nonlinear iteration method (a) radial wind speed; (b) backscatter ratio.

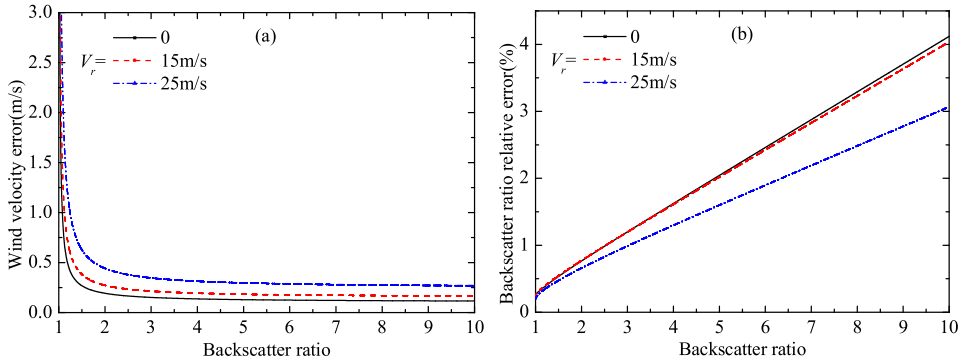

Fig. 9. (a) Radial wind speed measurement error and (b) Backscatter ratio measurement error vs backscatter ratio.

the wind speed. The smaller the R_β is, the faster the backscatter ratio converges; the larger the R_β, the slower the backscatter ratio converges.

4.3. Measurement error analysis

According to the error transfer formula, the measurement errors of radial wind speed and backscatter ratio obtained by Eq. (16) are

$$\varepsilon_V = \frac{\sqrt{\theta_{R1}^2 SNR_2^{-2} + \theta_{R2}^2 SNR_1^{-2}}}{\left|\theta_{V1}\theta_{R2} - \theta_{R1}\theta_{V2}\right|} \tag{17}$$

$$\varepsilon_R = \frac{\sqrt{\theta_{V1}^2 SNR_2^{-2} + \theta_{V2}^2 SNR_1^{-2}}}{\left|\theta_{V1}\theta_{R2} - \theta_{R1}\theta_{V2}\right|} \tag{18}$$

where SNR_1, SNR_2 are the signal to noise ratios of measuring h_{e1} and h_{e2} respectively. In the case of shot noise limit, we have

$$SNR_i = \left[\frac{1}{N_{0i}}\left(\frac{1}{\Im_{ei}} + \frac{1}{\Re_{ei}}\right)\right]^{-1/2} \tag{(19)}$$

where i = 1, 2; N_{0i} is the total number of backscattering photons received by the telescope.

When N_{0i} = 50,000, the radial wind speed measurement error and the backscatter ratio relative measurement error varying with the backscatter ratio at different radial wind speeds are shown in Fig. 9(a) and (b), respectively. It can be seen from Fig. 9(a) that the measurement error of radial wind speed decreases rapidly with the increase of R_β when $1<R_\beta<2$ and decreases slowly with the increase of R_β when $R_\beta>2$; when $R_\beta>1.1$, within the wind speed dynamic range of ± 25m/s, the radial wind speed error is less than 2m/s. As can be seen from Fig. 9(b), the relative measurement error of backscatter ratio increases as the backscatter ratio increases, and the relative error of backscatter ratio is less than 4.1% in the range of $1<R_\beta<10$.

5. Conclusion

In this paper, the data inversion method of the dual-frequency Doppler lidar based on FPE quad-edge technique is studied. The calibration method of the ratio function of FPE's transmission to reflection is given and its feasibility is verified. Based on the definition of the effective ratio function of FPE's transmission to reflection, a nonlinear iterative method is proposed to simultaneously retrieve wind speed and backscatter ratio. Simulation results show that no matter whether backscatter ratio is small or large, within the wind speed dynamic range of ± 25m/s, this method can always simultaneously and accurately retrieve the wind speed and the backscatter ratio, but only a slight difference in the speed of convergence. Further error analysis shows that when the total backscatter photon number is 50,000 and the backscatter ratio is between 1.1–10, the error of radial wind speed is less than 2m/s in the wind speed dynamic range of ± 25m/s, and the relative error of backscatter ratio is less than 4.1%. The relevant method proposed in the paper is also of great reference value for the inversion of multi-parameter detection lidar.

Acknowledgements

This work was supported by the Natural Science Foundation of Jiangsu Province, China (BK20161316), the Open Research Fund of Key Laboratory of Atmospheric Composition and Optical Radiation, Chinese Academy of Sciences (2017), the Young Scientists Fund of the National Natural Science Foundation of China (51504214) and National Science Foundation of the Higher Education Institutions of Jiangsu Province, China (17KJD240002).

References

[1] Z.S. Liu, B.Y. Liu, S.H. Wu, Z.G. Li, Z.J. Wang, High spatial and temporal resolution mobile incoherent Doppler lidar for sea surface wind measurements, Opt. Lett. 33 (13) (2008) 1485–1487.
[2] H.Y. Xia, X.K. Dou, D.S. Sun, Z.F. Shu, X.H. Xue, Y. Han, D.D. Hu, Y.L. Han, T.D. Cheng, Mid-altitude wind measurements with mobile Rayleigh Doppler lidar incorporating system-level optical frequency control method, Opt. Express 20 (14) (2012) 15286–15300.
[3] C. Souprayen, A. Garnier, A. Hertzog, A. Hauchecorne, J. Porteneuve, Rayleigh- Mie Doppler wind lidar for atmospheric measurements. I. Instrumental setup, validation and first climatological results, Appl. Opt. 38 (12) (1999) 2410–2421.
[4] B. Gentry, H. Chen, S.X. Li, Wind measurements with 355-nm molecular Doppler lidar, Opt. Lett. 25 (17) (2000) 1231–1233.
[5] M. Dehring, C. Nardell, J. Pavlich, P. Hays, I. Dors, Performance and comparison of 532nm and 355nm GroundWinds lidars, Proc. SPIE 4893 (2003) 337–347.
[6] O. Reitebuch, Ch. Lemmerz, E. Nagel, U. Paffrath, Y. Durand, M. Endemann, F. Fabre, M. Chaloupy, The airborne demonstrator for the direct-detection Doppler wind lidar ALADIN on ADM-Aeolus: I nstrument design and comparison to satellite instrument, J. Atmos. Ocean. Tech 26 (12) (2009) 2501–2515.
[7] R.M. Huffaker, A.R. Paul, Solid-state coherent laser radar wind field measurement systems, Pure Appl. Opt. 7 (1998) 863–873.
[8] S. Kameyama, T. Ando, K. Asaka, Y. Hirano, S. Wadaka, Compact all-fiber pulsed coherent Doppler lidar system for wind sensing, Appl. Opt. 46 (11) (2007) 1953–1962.
[9] F.H. Shen, A.A. Yu, J.H. Dong, Y.Q. Xia, C.L. Liu, Dual-frequency quad-edge frequency discrimination photoelectric detection technique based on single F-P etalon, Acta Optica Sin. 34 (3) (2014) 0312005.
[10] F.H. Shen, Y.Q. Xia, A.A. Yu, C.L. Liu, Research on dual-frequency Doppler lidar based on Fabry-Perot etalon quad-edge technique, Acta Optica Sin. 34 (10) (2014) 1001002.
[11] T.T. Kajava, H.M. Lauranto, R.R.E. Salomaa, Fizeau interferometer in spectral measurements, J. Opt. Soc. Am. B 10 (1993) 1980–1988.
[12] F.H. Shen, D.S. Sun, C.L. Liu, C.Q. Qiu, Z.F. Shu, Data inversion technique for single F-P etalon-based dual-frequency Doppler lidar, Acta Optica Sin. 62 (22) (2013) 220702.